Chemical Science

ROYAL SOCIETY OF CHEMISTRY

EDGE ARTICLE

View Article Online
View Journal | View Issue

Cite this: *Chem. Sci.*, 2026, **17**, 5542

All publication charges for this article have been paid for by the Royal Society of Chemistry

Molecular dynamics study of catalytic H_2/O_2 recombination on Pd, Pt, Cu, Ag, and Au nanoclusters using the universal neural network potential

Yusuke Tateishi, [ab] Louise M. Botha, [b] Alina E. Kozhukhova, [b] Manabu Sugimoto, *[ac] Ken-ichi Aika [d] and Dmitri G. Bessarabov *[b]

The H_2/O_2 catalytic recombination reaction, essential for safely utilizing hydrogen energy, was simulated rapidly and accurately using the molecular dynamics (MD) simulation with a machine-learning potential known as the 'universal neural network potential' (UNNP). The catalytic activities of Pd, Pt, Cu, Ag, and Au nanoclusters were systematically investigated under a 100 bar H_2/O_2 atmosphere at 500 K. This approach enables the investigation of the entirely dynamic catalytic reaction, rather than assembling a static configuration at 0 K. Throughout the simulation, the ability to catalyze H_2O formation on the Pt surface was successfully reproduced, aligning with previous experimental findings. The simulations have revealed characteristic differences and the suitability of reactivity with H_2/O_2 across the studied metals, demonstrating the time evolution of gas-surface interactions and the overall detailed reaction mechanism of the H_2/O_2 recombination reaction. In particular, the reaction pathway $O_2 \rightarrow OOH \rightarrow H_2O$ was revealed to occur preferentially on the Pt nanocluster, while other metals exhibited unsuitability, such as Pd's intense H trapping and Cu's surface instability due to excessive O_2 dissociation. The two features of molecular O_2 adsorption and the facile surface diffusion of H atoms play a crucial role as necessary conditions for catalytic activity. The accelerated MD method enables the rapid and accurate elucidation of the atomic-level mechanisms and activity differences in the H_2/O_2 recombination reaction, offering a fast and accurate workflow for both performance screening and mechanism discovery, thus accelerating catalyst design.

Received 26th June 2025
Accepted 23rd December 2025

DOI: 10.1039/d5sc04712a

rsc.li/chemical-science

1 Introduction

Green hydrogen, produced *via* electrochemical water splitting through water electrolysis powered by renewable energy sources, such as wind or solar, is widely regarded as a sustainable and environmentally friendly energy carrier. Once produced, hydrogen can be compressed, liquefied, or chemically converted into, for example, ammonia or liquid organic hydrogen carriers (LOHCs) such as methylcyclohexane (MCH) and perhydro-benzyltoluene (BT-H). Each of these options offers distinct advantages for hydrogen storage and long-distance transportation.[1] Additionally, green hydrogen can be combined with captured CO_2 to produce e-methane—a synthetic equivalent of natural gas—and it can be directly used as a carbon-neutral fuel, provided that the released CO_2 is subsequently captured and reused. Thus, green hydrogen plays a critical role in enabling the transition from fossil-based to sustainable energy systems.[2–4]

Despite its advantages, hydrogen presents safety challenges due to its low minimum ignition energy (0.02 mJ) and wide flammability range (4–75 vol% hydrogen in air).[5] Accidentally released hydrogen can rapidly move upwards, accumulate near ceilings, and mix with air in confined spaces. This, in turn, can lead to the formation of explosive mixtures, which, if ignited, will cause damage to infrastructure and loss of life. The accumulation of explosive hydrogen/air mixtures can occur in any confined space where hydrogen is used, such as garages for hydrogen-fueled cars, underground mines, fuel cell systems, and hydrogen storage facilities, including critical applications like nuclear power plants.

Various safety measures have been implemented to mitigate these risks, including the use of inert gases (*e.g.*, nitrogen, helium, and argon),[6] natural and forced ventilation,[7,8] water

[a]*Faculty of Advanced Science and Technology, Kumamoto University, 2-39-1 Kurokami, Chuo-ku, Kumamoto 860-8555, Japan*

[b]*HySA Infrastructure, North-west University, 11 Hoffman Street, Potchefstroom, 2531, South Africa. E-mail: Dmitri.Bessarabov@nwu.ac.za*

[c]*Department of Pharmaceutical Sciences, Daiichi University of Pharmacy, 22-1 Tamagawa-machi, Minami-ku, Fukuoka 815-8511, Japan. E-mail: m-sugimoto@daiichi-cps.ac.jp*

[d]*National Institute of Technology (KOSEN), Numazu College, 3600 Ooka, Numazu, Shizuoka 410-8501, Japan*

mists,[9] and the employment of safety devices such as passive autocatalytic recombiners (PARs).[1,5,10,11] Among these strategies, the use of PARs stands out as one of the most robust and widely adopted solutions. A PAR mitigates the risk of explosion by catalytically converting accidentally released hydrogen into water vapor through its reaction with oxygen present in the ambient air. The term "passive" refers to the ability to initiate the recombination reaction spontaneously as soon as hydrogen concentration begins to increase. Hence, PARs do not require any external power source.

Different types (catalysts) and models (dimensions and chimney) of PARs have been developed. The PAR manufacturers include Atomic Energy Canada Ltd (AECL), Electrowatt Engineering Ltd, NIS, Siemens, AREVA, Framatome, and ISPC RET. Typical catalytic materials include Pt- and Pd-coated plates, pellets, and rods. However, these catalysts face several challenges, including high material costs, overheating risks that may lead to self-ignition, and deactivation caused by exposure to water vapor and chemical poisons such as carbon monoxide and iodine.[12–14] The occurrence of hotspots on the catalyst surface can also lead to the self-ignition of the PAR due to the local initiation of combustion waves or flames that can propagate through the hydrogen/air mixture, ultimately damaging the inside components as well as the outside of the PAR.[15] To solve the problems mentioned above, it is important not only to develop new advanced catalysts but also to design the catalyst structure as a functional component.[15,16]

Transition metals, particularly platinum group metals (PGMs), are essential catalyst materials due to their high activity and versatility, making them fundamental to the hydrogen economy. The interaction between reactants (H_2 and O_2) and transition metals is crucial in key chemical processes, including the oxygen evolution reaction (OER), the oxygen reduction reaction (ORR), and H_2/O_2 recombination.[3,17,18] These reactions typically follow adsorption–desorption mechanisms, where reactants bind to the catalyst surface and detach as products. Extensive experimental research has focused on designing H_2/O_2 recombination catalysts to develop materials with catalytic activity comparable to or exceeding that of PGMs.[11,19–28] Computational studies[29–31] have also investigated electronic, thermodynamic, and structural properties of catalysts, deepening our understanding of existing catalysts and providing valuable feedback for experimental research, which is crucial for advancing catalyst design.[32,33]

Despite these computational advances, most previous investigations have remained essentially static, restricted to a handful of predefined elementary steps on ideal surfaces explored at 0 K. Consequently, capturing the concerted adsorption, diffusion, and recombination events has been difficult, which governs catalyst performance under realistic conditions.

To address this, we have introduced high-speed, high-precision Density Functional Theory (DFT)-level Molecular Dynamics (MD) simulations at finite temperatures, aiming to advance this research field. So far, DFT and MD simulations have been widely used in catalyst design[29,30] to provide computational insights. While these methods are generally faster than experimental approaches, they can still be time-consuming, depending on the scope of the research. Recent advancements in machine learning (ML), which drive artificial intelligence (AI) technologies, have gained attention for accelerating computational research and reducing time requirements. These advancements have significantly impacted both academia and industry. ML models, such as neural network potentials (NNPs), can approximate the energies obtained from first-principles methods, like the DFT and Hartree–Fock (HF) methods, significantly faster (exceeding 10^5 fold) than direct calculations.[34–36] The application of NNPs has proven highly effective in accelerating catalyst development and advancing understanding of catalytic processes. One notable computation platform is Matlantis, which utilizes the Universal Neural Network Potential (UNNP). Current research focuses on leveraging the UNNP within MD simulations to discover next-generation, high-performance materials and to gain deeper insights into the underlying mechanisms.[37,38]

In this study, we investigate the catalytic properties of Pd, Pt, Cu, Ag, and Au in the dynamical H_2/O_2 recombination reaction at finite temperature using universal neural network potential-driven molecular dynamics (UNNP-MD). The findings offer valuable insights into the reaction mechanisms, and contribute to improving catalytic efficiency. Among the metals analyzed, Pt is reconfirmed as the most active catalyst, offering balanced O_2 adsorption and diffusivity of H atoms on the metal surface, which are key factors influencing catalytic performance. At the same time, the reliability and applicability of the UNNP-MD approach for catalyst development are examined and confirmed.

2 Computational method

The Universal Neural Network Potential (UNNP) was implemented using the Matlantis software package[36,39] from Matlantis Corp., utilizing the universal PreFerred Potential (PFP).

2.1 Structure modelling

The nanoclusters were obtained from the Atomic Simulation Environment (ASE) software package.[40] The nanocluster has an icosahedral morphology, preserving a high proportion of the (111)-like stable surface,[41] totaling 309 atoms and a diameter of about 1 nm. Geometric optimizations of these were performed using the UNNP.

To simulate the catalytic H_2/O_2 recombination on these nanoclusters, the nanoclusters were embedded in a cubic unit cell, surrounded by H_2 and O_2 molecules, as shown in Fig. 1. Using this approach and structure, we simulated the catalytic performance of the nanoclusters in an H_2/O_2 environment.

2.2 Molecular dynamics simulation

The MD simulations were performed under an NVT ensemble using the Nosé–Hoover thermostat,[42,43] with a thermostat time constant (τ) of 10 femtoseconds (fs), retrieving force and potential energy determined by the UNNP. The temperature was fixed at 500 K, and the volume was set to 125 000 Å^3. The

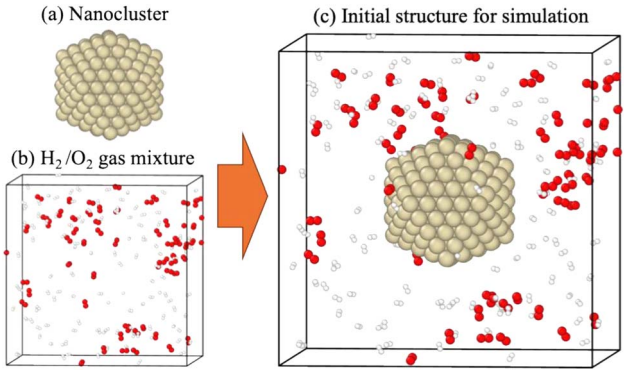

Fig. 1 The initial structure for the simulation. (a) An icosahedral nanocluster consisting of 309 atoms was inserted into (b) the H_2/O_2 gas mixture consisting of 117 H_2 and 58 O_2 molecules, where hydrogen and oxygen atoms were colored white and red, respectively. The initial structure (c) was generated by merging (a) and (b).

simulations were run for 200 picoseconds (ps), with a timestep of 1 fs. For each simulation, three runs were conducted, with the initial velocities of each atom randomly altered.

2.3 DFT calculation

The binding energies of hydrogen and oxygen on metal surfaces were investigated to validate the UNNP calculations. Spin-polarized plane-wave DFT calculations were performed using the Vienna *Ab Initio* Simulation Package (VASP).[44] The parameters selected for the DFT calculations were kept similar to those defined for the UNNP, which is applied using the Matlantis software.

3 Results and discussion

3.1 Characterization of metal surfaces in a H_2/O_2 gas mixture

Molecular dynamics (MD) simulations were conducted over 200 ps to investigate the catalytic performance of metal nanoclusters in the H_2/O_2 recombination reaction. The 200 ps MD simulation, which included 484 atoms, required only about 6–7 hours. As shown in Fig. 2, structural changes in metal nanoclusters after the 200 ps simulation were clearly observed. The initial nanoclusters shown in Fig. 2(a–e) have uniform surfaces without absorbents; in contrast, the structures in Fig. 2(a–e)′ captured several types of absorbents, indicating their characteristics and potential in the H_2/O_2 recombination reaction. Given the difference in reactivity and adsorption characteristics, these metal nanoclusters can be classified into three classes: (I) Pd and Pt, (II) Cu, and (III) Ag and Au.

Class I metals (Pd and Pt) facilitate the dissociative adsorption of hydrogen, leading to a rapid increase in H* species at the beginning of the simulation, as shown in Fig. 2(a and b). Here * denotes a species adsorbed on the metal surface. Interestingly, O_2 was preferentially adsorbed rather than atomic O. On Pd and Pt, O_2 molecules were primarily located at on-top/on-top sites, as shown in Fig. 2(a and b), suggesting that O_2 dissociation does not easily occur on these surfaces. Hydrogen atoms on the Pd surface tend to localize on hollow sites or migrate into the nanocluster, whereas H* is found on top or bridge sites on Pt. The adsorption characteristics of these PGMs, which are required for subsequent reactions, are clearly reflected in the atomic configurations, as shown in Fig. 2(a and b)′.

In contrast, Class II metal (Cu) exhibited significantly lower reactivity and was less suitable as a recombination catalyst. The Cu nanocluster showed strong interactions with oxygen, leading to substantial O_2 dissociation (Fig. 2(c)′). This resulted in a roughened surface and a lack of H and H_2 adsorption, suggesting that, under the given simulation conditions, the Cu surface is unstable, making it unsuitable as an H_2/O_2 recombination catalyst.

Class III metal (Ag and Au) nanoclusters were nert toward H_2, with only limited dissociative adsorption observed over time. Ag could adsorb molecular O_2 along with a small amount of dissociated H, whereas Au displayed even lower reactivity, with only minimal surface-bonded O_2 and H. These adsorption

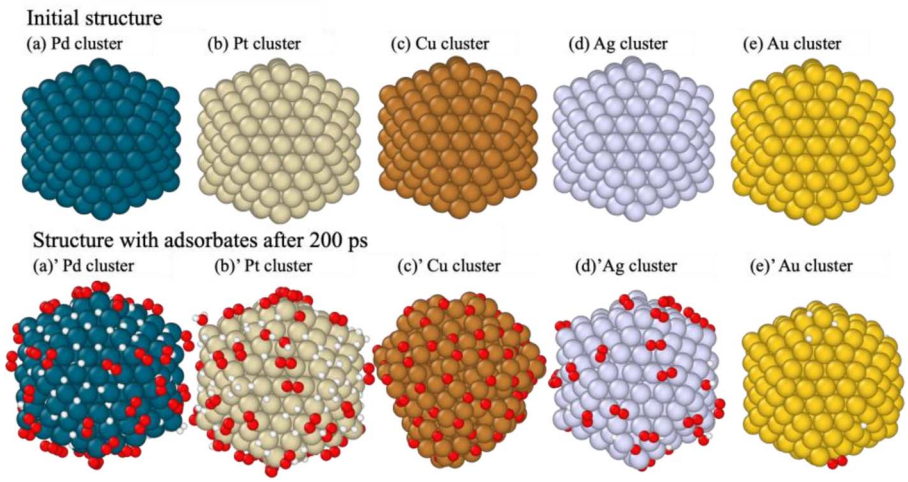

Fig. 2 Structures of metal nanoclusters before/after 200 ps simulation in a H_2/O_2 gas mixture (1st run). The first labeled (a), (b), (c), (d), and (e) represent the initial structures of Pd, Pt, Cu, Ag, and Au clusters, respectively. The lower panel: (a)′, (b)′, (c)′, and (d)′ shows the simulated structures after the MD simulation, with absorbates present on the surfaces.

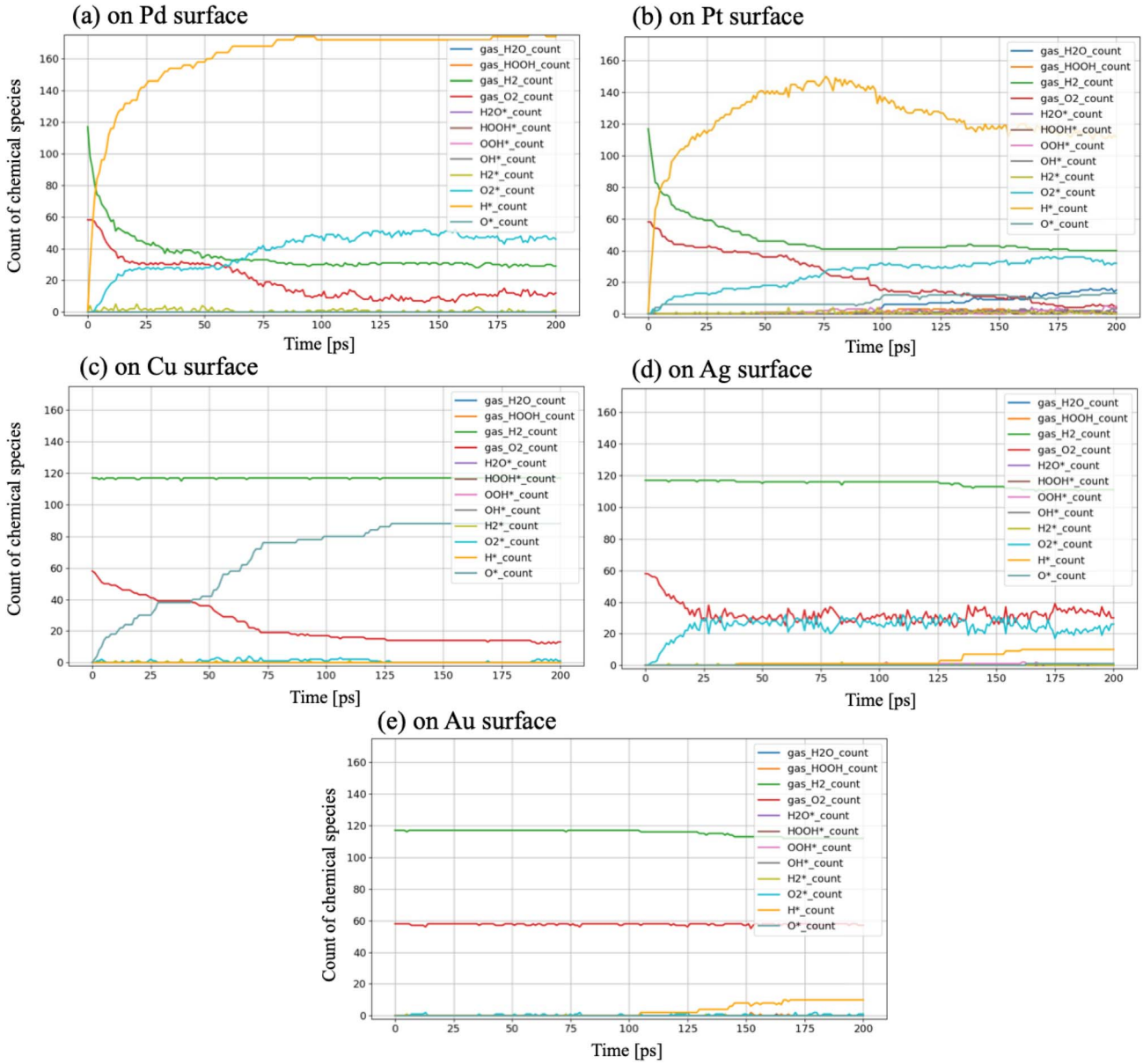

Fig. 3 Time evolution of chemical species obtained by simulation of the metal + H_2/O_2 system (1st run). "*" indicates a surface where species are adsorbed. (a), (b), (c), (d), and (e) are the reaction appearances on the Pd, Pt, Cu, Ag, and Au surfaces. The reproducibility of these MD results and the temperature dependence of the adsorption reaction and H_2O generation are discussed in the SI (Fig. S2 and S3).

behaviors, visualized in Fig. 2(d and e)′, support the conclusion that noble metals such as Ag and Au are less effective for catalytic recombination. At the same time, Pt and Pd were emphasized as offering favorable surface characteristics, leading to better H_2/O_2 recombination catalysts.

The atomic diffusion dynamics of oxygen and hydrogen atoms were also analysed based on the MD simulation trajectory. The following section discusses these findings in detail.

3.2 Reaction dynamics of chemical species (reactants, intermediates, and products)

As presented in Fig. 3 and Table 1, the number of chemical species, which can be categorized as reactants, intermediates, or products, was tracked and quantified, thereby identifying the chemical bonds between these species and metal surfaces. Fig. 3 illustrates the simulated time evolution of surface adsorption and reactions. Based on these observations, the following series of elementary reactions ((R1)–(R11)) can be presumed for the H_2/O_2 recombination process.

$$H_{2\ (gas)} \rightarrow H^* + H^* \quad (R1)$$

$$O_{2\ (gas)} \rightarrow O^* + O^* \quad (R2)$$

$$O_{2(gas)} \rightarrow O_2^* \quad (R3)$$

$$O^* + H^* \rightarrow OH^* \quad (R4)$$

Table 1 The average number of formed chemical species (reactants, intermediates, and products) and their standard deviation throughout the three 200 ps simulations. "*" indicates that the chemical species is adsorbed on a surface of the metal cluster. A value in parentheses indicates the standard deviation across three MD trajectories

	Reactants				Intermediates				Products	
Metal	O_2^*	H_2^*	O*	H*	OH*	OOH*	H_2O*	HOOH*	$H_2O_{(gas)}$	$HOOH_{(gas)}$
Pd	48 (1)	1 (0)	1 (1)	171 (8)	0 (0)	0 (0)	0 (0)	0 (0)	0 (0)	0 (0)
Pt	32 (2)	0 (0)	11 (2)	113 (4)	2 (2)	4 (1)	3 (2)	1 (1)	15 (2)	1 (0)
Cu	1 (1)	0 (0)	90 (2)	0 (0)	0 (0)	0 (0)	0 (0)	0 (0)	0 (0)	0 (0)
Ag	23 (2)	0 (0)	4 (2)	6 (3)	3 (1)	0 (0)	0 (0)	0 (0)	0 (0)	0 (0)
Au	0 (0)	0 (0)	0 (0)	5 (4)	0 (0)	0 (0)	0 (0)	0 (0)	0 (0)	0 (0)

$$O_2^* + H^* \rightarrow OOH^* \quad (R5)$$

$$O_2^* + 2H^* \rightarrow HOOH^* \quad (R6)$$

$$HOOH^* \rightarrow 2OH^* \quad (R7)$$

$$OH^* + H^* \rightarrow H_2O^* \quad (R8)$$

$$OOH^* + H^* \rightarrow OOH_2^* \quad (R9)$$

$$OOH^* \rightarrow OH^* + O^* \quad (R10)$$

$$OOH_2^* \rightarrow H_2O^* + O^* \quad (R11)$$

$$H_2O^* \rightarrow H_2O_{(gas)} \quad (R12)$$

$$HOOH^* \rightarrow HOOH_{(gas)} \quad (R13)$$

where * donates a species adsorbed on a metal surface.

Chemical bonds were identified when the distance between atoms was less than the sum of the covalent bond radii of each element pair.[45] Some example criteria used to classify each adsorbed species are as follows:

• $H_2O_{(gas)}$: one oxygen atom is bonded to two hydrogen atoms, with no metal atoms within the covalent bond radii of these atoms.

• $H_2O_{2(gas)}$: two connected oxygen atoms, each bonded to one hydrogen atom, with no metal atoms within the covalent bond radii of these atoms.

• O_2^*: two oxygen atoms are bonded, and at least one oxygen is bound to a metal atom within the covalent bond radii.

• OH*: an oxygen atom is bonded to a hydrogen atom and in contact with a metal atom within the covalent bond radii.

The quantity of all the reactants (H_2, O_2, H_2^*, O_2^*, H*, and O*), the intermediates (OH*, OOH*, H_2O*, and HOOH*), and the products (H_2O and HOOH), was determined using a consistent classification method. Regarding H_2O and HOOH, H_2O and HOOH are loosely bound to chemicals (not metals) on surfaces due to interactions such as hydrogen bonding or dispersion forces; however, those products have been counted as H_2O, and not H_2O*, because of any interaction with metal.

As shown in Fig. 3, adsorption in the system reaches convergence within 200 ps and reveals different features as catalysts, indicating that the chosen simulation time window is suitable to scope them, although the reaction of Pt is still ongoing towards producing H_2O, as visible in Fig. S4. The temporary quantities of the chemical species, and their standard deviation after three 200 ps runs are summarized in Table 1. Based on these data, the following unique features were quantitatively identified.

3.2.1 Class I metals: Pt and Pd. Regarding Class I metals, the Pd surface exhibited limited catalytic reactivity while demonstrating an ideal capacity for capturing hydrogen and oxygen. As shown in Fig. 3(a), dissociative adsorption of hydrogen proceeded rapidly (R1), with H atoms strongly trapped in hollow sites. In contrast, O_2 adsorption occurred dominantly without O_2 dissociation (R3), highlighting Pd's limited oxidization properties. This behavior suggests that while Pd has a strong affinity for capturing both H_2 and O_2, it lacks the necessary reactivity to progress toward formation of intermediates such as OH*.

As shown in Table 1, no products or intermediates were observed in this 200 ps simulation on the Pd surface. However, Pd has been recognized experimentally as an active metal in the H_2/O_2 recombination reaction as PdO[21] or PdO_x/γ-Al_2O_3.[22] And there are also DFT studies demonstrating the H_2O and H_2O_2 formation mechanism of Pd, depending on O_2 adsorption.[46,47] This discrepancy between previous studies and our result: Pd's low catalytic activity is possibly due to several conditional limitations: the system's high temperature, non-lean hydrogen, non-surface oxidization, the absence of a support, *etc.*[22] The lack of activity in the recombination reaction should be the result of the combined effects of excessive O_2 and H adsorption, affected by the above points. These findings highlight Pd's potential in H_2/O_2 recombination but emphasize the need for structural or alloying modifications to overcome its limitations in H_2/O_2 recombination reactions.

Regarding another Class I metal, 15 H_2O molecules were produced during the simulation, along with surface-bound intermediates such as OOH*, OH*, and H_2O*, as evidenced in Table 1. Similar to Pd, it demonstrated that O_2 and O adsorption can occur on the Pt surface ((R2) and (R3)). From Fig. 3(b), on the Pt surface, H_2 dissociation and H adsorption (R1) began intensely at the start of the simulation. Subsequently, a decrease in adsorbed hydrogen atoms was observed, and the formation of intermediates began at around 75 ps. Notably, as shown in Fig. 4(a), significantly larger amounts of OOH* were formed in comparison to OH*. This observation suggests that the

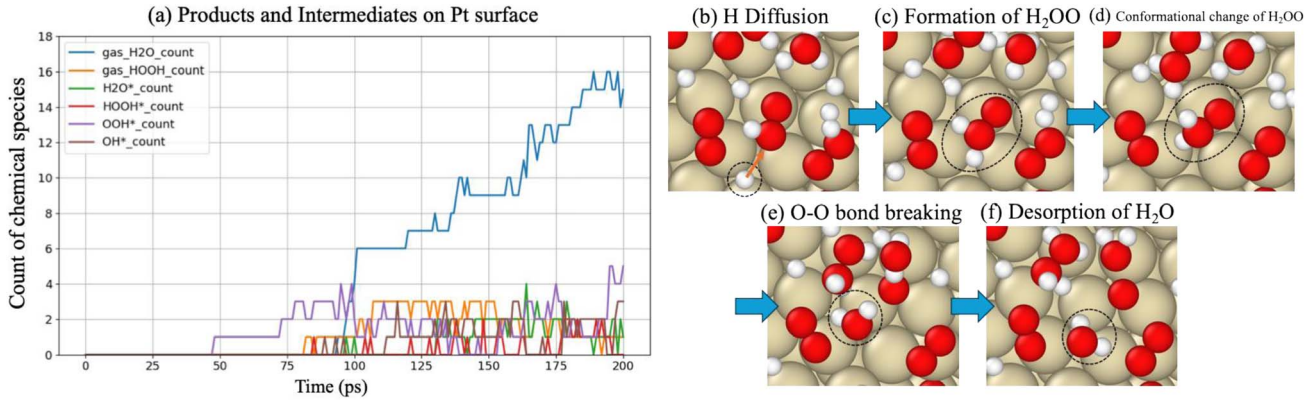

Fig. 4 Forming intermediates and products. (a) More detailed reaction time evolution (than Fig. 3(b)), specifically intermediates and products on the Pt surface. Snapshot of the simulated reaction forming H_2O from OOH* and H* on the Pt surface. (b) The presence of OOH* and atomic H*. (c) OOH_2^* is formed through the bonding of H* with OOH*. In (d), a conformational rearrangement occurs. (e) The dissociation of OOH_2^* into H_2O and another product. Finally, H_2O is desorbed from the surface into air, as shown in (f).

formation of H_2O does not originate primarily from OH* (R8) but rather from a reaction sequence following O_2 adsorption and OOH* formation on the Pt surface (R5).

Furthermore, when comparing the O_2 adsorption capacities of Pd and Pt, it is evident that Pt has a slightly lower adsorption capacity (Table 1). The difference suggests that Pt's moderate Pt–OO–Pt interaction strength creates an ideal environment for forming intermediates such as OOH* and OH* ((R5) and (R6)).

As shown in Fig. 4(b–f), O_2 adsorbed on the Pt surface combined with H to produce OOH*, which led to the formation of the target product, H_2O. This reaction pathway is consistent with the mechanism demonstrated by Jacob's DFT study,[48] in which H_2O was produced *via* OOH*. The O_2 adsorption likely serves as a critical initial state, enabling subsequent reaction steps ((R8) and (R9)), through forming key intermediates such as OH* and OOH*.

Among Class I metals, Pt exhibited optimal balance between O_2 adsorption and mobility for hydrogen, making it the most effective catalyst in H_2/O_2 recombination. As presented in Fig. 3, Pt has adsorbed a moderate number of H* species—more than Cu or Ag but fewer than Pd—indicating Pt's moderate H* adsorption strength. As will be discussed in detail later, this adsorption property ensures sufficient surface mobility of hydrogen, which is essential for subsequent reactions leading to H_2O and H_2O_2 formation, creating an optimal environment for catalytic activity for H_2/O_2 recombination. The balance of two requirements, which are O_2 adsorption and mobility for hydrogen, facilitated efficient reaction progression, leading to the formation of 15H_2O molecules and intermediates such as H_2O*, OOH*, and OH* (Table 1).

3.2.2 Class II metal: Cu. On the other hand, a Class II metal, Cu, adsorbed only O atoms without H adsorption, indicating its strong O_2 dissociation ability. The adsorbed O* seems to strongly interact with surface Cu atoms because appreciable surface reconstruction is observed as shown in Fig. 2(c)′. H_2 adsorption and dissociation were rarely observed, suggesting that Cu has a weak interaction with hydrogen. This observation is consistent with its lower hydrogen binding energy[49] compared to Pd and Pt. As shown in Fig. 3(c), the amount of O adsorption steadily increased (R2), and by around 200 ps, adsorption reached a plateau. As indicated by the green line, no hydrogen adsorption occurred at any point during the simulation. Consequently, the excessively strong Cu–O interaction, combined with the absence of H adsorption, renders Cu impractical as a catalyst for the H_2/O_2 recombination reaction. However, its strong O_2 dissociation ability highlights its potential for oxidation-specific reactions.[50]

Although a pure Cu nanocluster appeared catalytically inactive in our simulations, it is known that oxidized copper species (CuO) exhibit catalytic activity in experimental H_2/O_2 recombination.[21] In our model and approach, partial oxidation of the Cu surface was observed; however, a fully oxidized CuO surface was not explicitly constructed or simulated due to the limited O_2 gas supply and simulation time. This discrepancy highlights a limitation of our computational approach to catalytic reactions, including the surface oxidation process. To simulate the reaction for metal oxides such as PdO and CuO, computationally, prior oxidation treatment should be required.

3.2.3 Class III metals: Ag and Au. For Class III metals, on the Ag surface, moderate O_2 adsorption occurred (R3), accompanied by a small amount of hydrogen adsorption and dissociation (R1). Thereafter, the formation of a few OH* was observed, as shown in Table 1. Although Ag facilitated some key reaction steps in the recombination process, no H_2O formation was observed. Moreover, given weak adsorption energies,[49] the overall catalytic efficiency for Ag likely remains low. It is worth noting that Ag is a well-established catalyst for ethylene epoxidation, where molecular O_2 is activated to the intermediates (Ag–O–O*) on the surface.[51] The presence of O_2^* in our simulations supports the validity of our approach and observation. These results suggest that while Ag exhibits moderate catalytic activity, further optimization, such as alloying, is necessary for enhancing its performance in H_2/O_2 recombination reactions.

The Au surface exhibited minimal catalytic activity, with non-aggressive adsorption and surface reactions, except for a small amount of H adsorption. A previous study[52] also

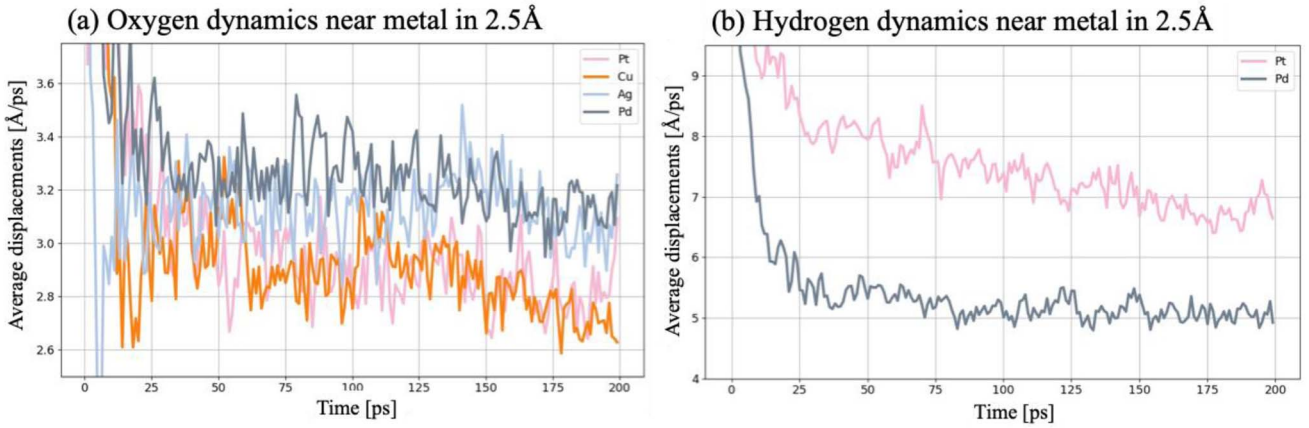

Fig. 5 Time evolution of the adsorbate-averaged displacement (per 1 ps). (a) Average displacement of oxygen atoms adjacent to the metal nanocluster. (b) Average displacement of hydrogen atoms adjacent to the metal nanocluster.

demonstrated that hydrogen interacts and dissociates on Au nanoclusters. These results suggest that Au's surface characteristics are inherently unsuitable for H_2/O_2 recombination reactions despite its application in other catalytic processes, such as CO oxidation.[53] Moreover, the low binding energies for both H and O suggest that adsorption will not readily occur on the Au surface, which aligns with the general properties of Au. Utilizing Class III metals in H_2/O_2 recombination reactions is challenging, but these properties possibly suppress the overly strong interactions of other elements through alloying, like the development of Pd–Au.[54]

Overall, Pt exhibited the highest catalytic performance, reaffirming its superiority as an ideal catalyst for the H_2/O_2 recombination reaction. The exceptional catalytic activity of Pt has been well-established in previous studies,[5,6,24–30] and the present simulations further validate these findings. Fig. 3(b) and 4(a) highlight Pt's superior performance, which stems from its unique combination of adsorption properties. Specifically, the findings suggest that an effective H_2/O_2 recombination catalyst relies not on strong O_2 dissociation but on efficient O_2 adsorption and the facilitation of moderate-strength H adsorption, which leads to OOH* formation, as shown in Fig. 4.

In this study, we have investigated the catalytic reactivity of icosahedral nanoclusters for the five metals. They are mainly covered by the (111) surfaces. It should be noted that catalytic activity may vary in other symmetries with different types of exposed surfaces and edges. The influence of alternative morphologies, including truncated octahedra and decahedra, should also be investigated in future studies.

3.3 Diffusion of oxygen and hydrogen on metal surfaces

The previous section established that the efficiency of O_2 adsorption plays a critical role in catalytic H_2/O_2 recombination. Therefore, this section analyzes the displacement behavior of oxygen and hydrogen on the nanoclusters to gain insights into the dynamic behavior of the adsorbates on the surfaces. At this time, the oxygen and hydrogen being analyzed are limited to those within 2.5 Å of metal atoms. This is to prevent the overestimation of displacement caused by oxygen and hydrogen in air.

Fig. 5(a) illustrates the varying displacement behaviors of oxygen on each metal surface. As described above (Fig. 2(a, b and d)), on Ag, Pt, and Pd surfaces, oxygen typically exhibited O_2 adsorption, while Cu formed a strong Cu–O bond. Oxygen displacement on Ag and Pd surfaces is relatively similar, at around 3.2 Å ps^{-1}, compared to restricted oxygen displacement of Pt of around 2.9 Å ps^{-1}. This difference indicates that O_2 on the Pt surface is more stable and strongly adsorbed compared to Ag and Pd. The displacement of Cu is smaller than that of Ag and Pd, and its displacement is nearly equivalent to that of Pt, suggesting that oxygen atoms are strongly adsorbed on the Cu surface and their movement is restricted. Fig. 5(b) illustrates the difference in hydrogen diffusion properties between Pt and Pd. The average hydrogen displacement on the Pt surface is around 6.5–7.0 Å ps^{-1}, which is significantly larger than that on Pd, at approximately 5.0 Å s^{-1}. This suggests that hydrogen diffuses more easily on the Pt surface than on Pd, affecting the differences in accessibility to oxygen toward subsequent reactions.

The analysis of dynamic diffusion showed that Pt retains O_2 on the surface with moderate strength while also facilitating the diffusion of dissociated hydrogen. In contrast, although Pd can adsorb both O_2 and dissociated hydrogen, H diffusion on the Pd surface was more restricted. For the development of catalysts with performance comparable to Pt, a key strategy may involve weakening Pd's O_2 adsorption ability and enhancing its H diffusion properties through alloying, thereby creating an environment similar to that of Pt.

3.4 Comparisons with DFT calculations

Finally, we briefly compared the validity of the UNNP with DFT and experimental values. The surface slab model was used to investigate the H and O adsorption structures and binding energy with the metal.

The bulk structures of Pd, Pt, Cu, and Au belong to the $Fm\bar{3}m$ space group and thus adopt a face-centered cubic (FCC) crystal structure. In contrast, Ag belongs to the $P6_3/mmc$ space group,

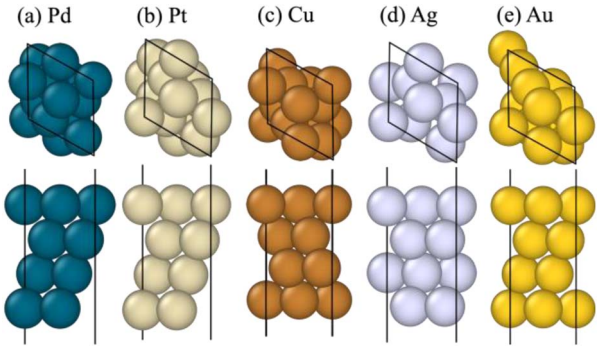

Fig. 6 Surface slab models of (a) Pt, (b) Pd, (c) Cu, (d) Ag, and (e) Ag generated from the single crystals—upper: top view; lower: side view.

corresponding to a hexagonal close-packed (HCP) crystal structure at room temperature.

For the crystal surfaces, the (111) surface was used for FCC structures, while the (0001) surface was used for the HCP structure. Among various adsorbates, we focus on atomic H and O on the Pt, Pd, Cu, Au, and Ag surfaces. The optimized slab structures are summarized in Fig. 6. The constructed surface slabs had a (2 × 2) surface area with four layers, totaling 16 atoms. A vacuum gap of 12 Å was added between vertically repeating slabs to ensure sufficient separation between periodic cells and minimize interactions.

3.4.1 Bond lengths of O* and H* to metal surfaces. Although numerous adsorption sites and modes may exist, this section focuses on atomic H and O as adsorbates on Pt, Pd, Cu, Au, and Ag surfaces. A comprehensive analysis and verification of all possible adsorption sites and modes is beyond the scope of this study. Previous research has shown that hollow sites—particularly three-fold fcc and hcp sites—are among the most stable adsorption sites for atomic H and O on many transition metal surfaces.[49,50,55–58] Applying the UNNP, we identified adsorbed atomic species at these sites, as illustrated in Fig. 7. These structures were also optimized using DFT calculations. The two methods produced consistent Pd–X distances (X = H or O), with deviations from DFT of less than 0.73%. Similar levels of agreement were observed for the other metal surfaces (Fig. S6 and S7), demonstrating that the UNNP reliably reproduces the atomic geometries of adsorbed species on the metal surfaces investigated in this study.

3.4.2 Binding energy of O* and H* to metal surfaces. We also evaluated the binding energies of the atomic species discussed above. The binding energy (E_{bind}) of the adsorbed species was calculated using the following equation:

$$E_{bind} = (E_{slab} + E_{adsorbent,isol}) - E_{(slab+adsorbent)} \quad (1)$$

where ($E_{slab+ads}$) is the total energy of the optimized surface with the adsorbate, (E_{slab}) is the energy of the clean metal surface, and ($E_{ads,isol}$) is the energy of the isolated adsorbate in the gas phase.

Binding energy is a key parameter for understanding the interaction between adsorbates and the surface, providing insights into adsorption strength and surface reactivity. In general, higher binding energies (more positive values) indicate a stronger interaction between the adsorbent and the surface. However, if the binding is too strong, it may hinder subsequent reaction steps—an outcome described by the Sabatier principle.[59] The UNNP-based binding energies are summarized in Table 2, together with the DFT results and experimental values. When comparing the binding energies of O and H on the slab surfaces of Pd, Pt, Cu, Ag, and Au, noticeable differences are likely observed in each metal's adsorption capability and reactivity. The additional comparison results with some other DFT studies are shown in Table S1.

3.4.3 Oxygen binding. Regarding binding energy with oxygen, Pd and Pt showed moderate binding energies and characteristics. Specifically, Pd had a binding energy of 412.96 kJ mol^{-1} at the face-centered cubic (fcc) site and 407.17 kJ mol^{-1} at the hexagonal close-packed hcp site, while Pt had a binding energy of 379.19 kJ mol^{-1} at the fcc site and 367.61 kJ mol^{-1} at the hcp site. This trend has been consistent for both DFT and experimental values, with an energy difference of less than 38 kJ mol^{-1} (0.4 eV). Cu exhibited the strongest binding strength, with values of 448.66 kJ mol^{-1} at the fcc site and 445.76 kJ mol^{-1} at the hcp site, indicating that O_2 is expected to dissociate efficiently on the surface. Weaker binding was observed on the Ag surface, with energies of 345.42 kJ mol^{-1} at the fcc site and 343.49 kJ mol^{-1} at the hcp site. Binding energies with oxygen on the Au slab surface were the smallest, with values of 2.64 kJ mol^{-1} at the fcc site and 340.59 kJ mol^{-1} at the hcp site. Among the five metals investigated, Au exhibited the lowest binding energy, indicating that O adsorption is unlikely to occur on its surface. For Cu, Ag, and Au, the difference between the UNNP, DFT, and experimental binding energies ranged from approximately 1 to 10 kJ mol^{-1}.

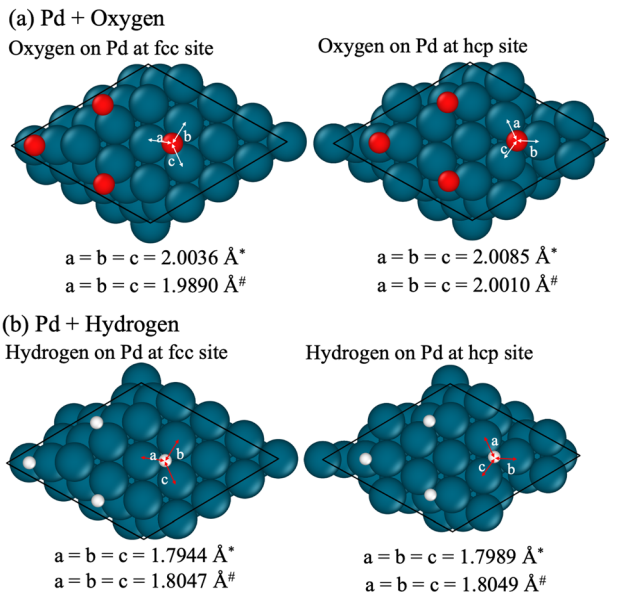

Fig. 7 As an example, adsorbed structures of (a) Pd slab with O* and (b) Pd slab with H*, where * and # indicate values calculated with the UNNP and DFT. These structures are expanded to 2 unit cells for the *x*-axis and *y*-axis.

Table 2 Calculated binding energies (kJ mol^{-1}) with O and H for Pt, Pd, Cu, Ag, and Au metals using the UNNP and DFT-based geometry optimization

		Pd		Pt		Cu		Ag		Au	
X	Site	UNNP	DFT	UNNP	DFT	UNNP	DFT	UNNP	DFT	UNNP	DFT
O	fcc	412.96	401.38	379.19	367.61	448.66	445.76	345.42	343.49	254.72	258.58
	hcp	407.17	380.15	367.61	330.94	442.87	434.18	340.59	333.84	246.04	242.18
	Exptl.	n.d.		357.00[a]		443.83[b]		331.91[c]		234.46[d]	
H	fcc	279.81	274.98	274.02	257.62	245.07	241.21	210.34	212.27	200.69	203.58
	hcp	279.81	268.23	274.98	254.72	243.14	241.21	208.41	211.30	197.79	201.65
	Exptl.	260.00[e]		268.23[f]		234.46[g]		176.57 to 192.97[h]		n.d.	

[a] Ref. 60. [b] Ref. 61. [c] Ref. 62. [d] Ref. 63. [e] Ref. 64. [f] Ref. 65. [g] Ref. 50. [h] Ref. 66.

3.4.4 Hydrogen binding. Regarding hydrogen binding energy, the Pd slab surface exhibited values of about 279.81 kJ mol^{-1} at both the fcc and hcp sites. For the Pt surface, the binding energies were 274.02 kJ mol^{-1} at the fcc site and 274.98 kJ mol^{-1} at the hcp site. According to the Sabatier principle, the moderate adsorption characteristics of Pt and Pd make them more favorable for surface adsorption and reactions involving hydrogen compared to other transition metals. The differences between the UNNP, DFT, and experimental values for Pd were about 20 kJ mol^{-1}, which may underestimate the ease of hydrogen diffusion. In any case, the lack of consistency between the binding energy in single-point calculations and the H* adsorption amount in the simulations is interesting. This inconsistency suggests that Pd enables the formation of solid-soluble hydrogen with hydrogen diffusion into the subsurface, and site competition has possibly occurred between O_2^* and H* on the Pt surface (Fig. 2(a, b)′ and S8).

In contrast, Cu showed weaker interaction with H, with binding energies of 245.07 kJ mol^{-1} at the fcc site and 243.14 kJ mol^{-1} at the hcp site, both lower than those of Pd and Pt. Similarly, Ag and Au demonstrate inactivity towards H adsorption, as reflected by their even lower binding energies: 208.41 to 210.34 kJ mol^{-1} for Ag and 197.79 to 200.69 kJ mol^{-1} for Au. Consequently, H adsorption is more challenging on these metal surfaces than on Pd and Pt surfaces. For Ag, the binding energy may have been overestimated relative to the experimental values; however, the overall accuracy of the UNNP predictions for Cu, Ag, and Au was assessed to be high.

Overall, the UNNP-MD simulations effectively estimated the catalytic activity of transition metals with both high computational efficiency and accuracy, yielding results consistent with experimental observations. The adsorption and reaction behaviors observed across the five metal surfaces offer valuable insights into their catalytic roles in the H_2/O_2 recombination reaction. These results suggest that designing catalysts with optimal O_2 adsorption properties and moderate H adsorption strength—allowing hydrogen to diffuse on the surface—could lead to efficient and cost-effective alternatives to Pt catalysts. One possible strategy to reduce Pt usage is to dilute Pt with relatively inert metals, such as Ag or Au, while maintaining the balanced interaction with H_2/O_2. In the case of Pd, which binds H strongly, introducing inert metals such as Au may weaken H adsorption and thereby enhance catalytic performance. The computational workflow and resulting insights offer a strategic foundation for alloying or surface engineering aimed at improving catalytic performance in H_2/O_2 recombination reactions.

4 Conclusions

This study simulated the dynamic adsorption process and their subsequent reactions in H_2/O_2 recombination at finite temperature, which is one of the key processes for ensuring hydrogen safety. Specifically, we examined the reaction activity on Pd, Pt, Cu, Ag, and Au on metal nanocluster surfaces, using universal neural network potential (UNNP)-based molecular dynamics (MD) simulations.

The UNNP approach successfully reproduced the adsorption energies of hydrogen and oxygen on each metal slab and its structure, with results showing good agreement with DFT results. Accelerated UNNP-MD simulations reaffirmed Pt as the most active catalyst surface for this reaction. These findings demonstrate that the UNNP approach is a practical and efficient tool for systematically evaluating catalytic activity in the H_2/O_2 recombination reaction.

Moreover, the simulations provided mechanistic insight, revealing that the catalytic activity of Pt is strongly related to the moderate-strength O_2^* adsorption as the initial step and the ease of hydrogen diffusion across the surface. In contrast, Pd captured both of these species more strongly than Pt, limiting their catalytic activity. These results highlight the importance of achieving a balance between adsorption strength and diffusion dynamics to optimize catalytic performance. Pt's exceptional performance enhances its role as a benchmark catalyst, while the limitations observed in Cu, Pd, and Ag suggest that performance enhancements may be achieved through alloying or surface engineering. Through specific alloying, maintaining or promoting selective O_2^* adsorption and hydrogen diffusion dynamics are expected to be important in reducing the practical cost of Pt. This exciting discovery has been obtained through dynamical H_2/O_2 recombination reactions at finite temperature, which is typically not achievable through DFT calculations based on single-molecule adsorption or predefined reaction models.

In summary, our approach has revealed the key factors required for the H_2/O_2 recombination reaction catalyst, referring to Pt's exceptional performance. Our *in silico* catalyst

screening studies are ongoing, and will be reported in future publications.

Author contributions

Y. Tateishi: conceptualization, methodology, computations, formal analysis, data curation, software development, visualization, validation, writing – original draft; L. M. Botha: DFT calculations, formal analysis, data curation, validation, writing – review & editing; A. E. Kozhukhova: writing – review & editing; M. Sugimoto: conceptualization, methodology, funding acquisition, project administration, supervision, writing – review & editing; K.-i. Aika: funding acquisition, project administration, resources, supervision, writing – review & editing; D. G. Bessarabov: funding acquisition, project administration, resources, supervision, writing – review & editing.

Conflicts of interest

There are no conflicts to declare.

Data availability

The detailed computational methods and supporting data are provided in the supplementary information (SI) and available from the present authors upon reasonable request. The scripts of simulation and data analysis are disclosed at [https://github.com/sugimoto-laboratory/h2o2_recombination/].

Supplementary information is available. See DOI: https://doi.org/10.1039/d5sc04712a. Trajectories in the MD simulations are available as MOV files.

Acknowledgements

This work was supported by JST/JICA, SATREPS (Science and Technology Research Partnership for Sustainable Development), "Development of new ammonia synthesis system using renewable energy and hydrogen" (JPMJSA2104) and by JST, BOOST (JPMJBS2408). In carrying out this research, we were greatly assisted by the staff of the HySA Infrastructure Center of Competence at North-West University (NWU), South Africa, and by JICA staff. We would also like to acknowledge the Centre for High-Performance Computing (CHPC) facility of South Africa in the completion of this work.

References

1 J. Kim, J. Yu, S. Lee, A. Tahmasebi, C. H. Jeon and J. Lucas, Advances in catalytic hydrogen combustion research: catalysts, mechanism, kinetics, and reactor designs, *Int. J. Hydrogen Energy*, 2021, **46**, 40073–40104.

2 S. Aslam, S. Rani, K. Lal, M. Fatima, T. Hardwick, B. Shirinfar and N. Ahmed, Electrochemical hydrogen production: sustainable hydrogen economy, *Green Chem.*, 2023, **25**, 9543–9573.

3 S. Karim, N. Tanwar, S. Das, R. Ranjit, A. Banerjee, N. Gulafshan, A. Gupta, A. Kumar and A. Dutta, Shaping the Future of Green Hydrogen Production: Overcoming Conventional Challenges with Molecular Catalysts, Immobilization, and Scalable Electrolyzers, *ACS Catal.*, 2025, **15**, 1073–1096.

4 S. Safari, F. Esmaeilion, A. Rabanian, D. H. Jamali, S. Negi, S. Hoseinzadeh, F. Sayedin, S. S. Bhoglla, M. El Haj Assad, B. Das, M. A. Ehyaei, A. Ahmadi, M. Soltani and H. Afshari, Sustainable hydrogen production through water splitting: a comprehensive review, *Environ. Dev. Sustain.*, 2025, **27**, 17887–17926.

5 A. E. Kozhukhova, S. P. du Preez and D. G. Bessarabov, Catalytic Hydrogen Combustion for Domestic and Safety Applications: A Critical Review of Catalyst Materials and Technologies, *Energies*, 2021, **14**, 4897.

6 P. Yang, T. Wang, Y. Sheng, Y. Yu, R. Li, B. Su, F. Cheng, J. Qu, J. Deng and Z. Luo, Recent advances in hydrogen process safety: Deflagration behaviors and explosion mitigation strategies, *Process Saf. Environ. Prot.*, 2024, **188**, 303–316.

7 A. A. Malakhov, A. V. Avdeenkov, M. H. Du Toit and D. G. Bessarabov, CFD simulation and experimental study of a hydrogen leak in a semi-closed space with the purpose of risk mitigation, *Int. J. Hydrogen Energy*, 2020, **45**, 9231–9240.

8 J. Lee, S. Cho, C. Park, H. Cho and I. Moon, Numerical analysis of hydrogen ventilation in a confined facility with various opening sizes, positions and leak quantities, *Comput. Aided Process Eng.*, 2017, **40**, 559–564.

9 Z. Wang, X. Gou, Q. Meng and H. Zhang, Effects of water sprays on hydrogen autoignition in heated air, *Process Saf. Environ. Prot.*, 2024, **192**, 915–925.

10 L. J. Yuan, Z. C. Zhao, W. Q. Wang, Y. F. Wang and Y. J. Liu, Review of Catalysts, Substrates, and Fabrication Methods in Catalytic Hydrogen Combustion with Further Challenges and Applications, *Energy Fuels*, 2024, **38**, 4881–4903.

11 A. E. Kozhukhova, S. P. Du Preez and D. Bessarabov, Preparation of Highly Active and Thermally Conductive Platinum Nano-particle/Ce–Zr–Y Mixed Oxide/AAO Washcoat Catalyst for Catalytic Hydrogen Combustion Technologies, *ACS Appl. Nano Mater.*, 2022, **5**, 8161–8174.

12 M. Klauck, E.-A. Reinecke, S. Kelm, N. Meynet, A. Bentaïb and H. J. Allelein, Passive auto-catalytic recombiners operation in the presence of hydrogen and carbon monoxide: Experimental study and model development, *Nucl. Eng. Des.*, 2014, **266**, 137–147.

13 M. Klauck, E.-A. Reinecke and H.-J. Allelein, Effect of par deactivation by carbon monoxide in the late phase of a severe accident, *Ann. Nucl. Energy*, 2021, **151**, 107887.

14 K. Inagawa, D. Matsumura, M. Taniguchi, S. Uegaki, T. Nakayama, J. Urano, T. Aotani and H. Tanaka, Development of Hydrogen Oxidation Reaction Catalysts to Overcome CO Poisoning and Elucidation of Reaction Mechanism, *J. Phys. Chem. C*, 2023, **127**, 11542–11549.

15 I. A. Kirillov, Passive Autocatalytic Recombiners as Explosion Prevention and Mitigation Tool in Hydrogen Energy and Transport Infrastructures, *Chem. Eng. Trans.*, 2022, **90**, 127–132.

16 P. Broeckerhoff, W. V. Lensa and E. A. Reinecke, Irregular thickness catalytic hydrogen recombination panel for water-cooled nuclear reactor minimizes the risk of fire and explosion, *Ger. Pat.*, DE19852953C1, 2000.

17 X. Gao, Y. Chen, Y. Wang, L. Zhao, X. Zhao, J. Du, H. Wu and A. Chen, Next-Generation Green Hydrogen: Progress and Perspective from Electricity, Catalyst to Electrolyte in Electrocatalytic Water Splitting, *Nano–Micro Lett.*, 2024, **16**, 237.

18 M. Awad, A. Said, M. H. Saad, A. Farouk, M. M. Mahmoud, M. S. Alshammari, M. L. Alghaythi, S. H. E. Abdel Aleem, A. Y. Abdelaziz and A. I. Omar, A review of water electrolysis for green hydrogen generation considering PV/wind/hybrid/hydropower/geo-thermal/tidal and wave/biogas energy systems, economic analysis, and its application, *Alex. Eng. J.*, 2024, **87**, 213–239.

19 J. Kim, S. Hong, K. H. Park, J. H. Kim and J. Y. Oh, Experimental Study on Hydrogen Recombination Characteristics of a Passive Autocatalytic Recombiner during Spray Operation, *Hydrogen*, 2022, **3**, 197–217.

20 K. C. Sandeep, R. Bhattacharyya, C. Warghat, K. Bhanja and S. Mohan, Experimental investigation on the kinetics of catalytic recombination of hydrogen with oxygen in air, *Int. J. Hydrogen Energy*, 2014, **39**, 17906–17912.

21 M. Haruta and H. Sano, Catalytic combustion of hydrogen I—Its role in hydrogen utilization system and screening of catalyst materials, *Int. J. Hydrogen Energy*, 1981, **6**, 601–608.

22 J. F. Kramer, S.-A. S. Reihani and G. S. Jackson, Low-Temperature Combustion of Hydrogen on Supported Pd Catalysis, *Proc. Combust. Inst.*, 2002, **29**, 989–996.

23 A. E. Kozhukhova, S. P. Du Preez, I. Shuro and D. G. Bessarabov, Preparation of a Cartridge-Type Pt/Al_2O_3 Catalyst Using a Sputter Deposition Method for Catalytic Hydrogen Combustion, *Energy Fuels*, 2022, **36**, 13911–13923.

24 A. E. Kozhukhova, S. P. Du Preez, A. A. Malakhov and D. G. Bessarabov, A Thermally Conductive Pt/AAO Catalyst for Hydrogen Passive Autocatalytic Recombination, *Catalysts*, 2021, **11**, 491.

25 A. E. Kozhukhova, S. P. Du Preez and D. G. Bessarabov, Development of $Pt–Co/Al_2O_3$ bimetallic catalyst and its evaluation in catalytic hydrogen combustion reaction, *Int. J. Hydrogen Energy*, 2024, **51**, 1079–1096.

26 A. E. Kozhukhova, S. P. Du Preez and D. G. Bessarabov, Preparation of Pt/Ce–Zr–Y mixed oxide/anodized aluminium oxide catalysts for hydrogen passive autocatalytic recombina-tion, *Int. J. Hydrogen Energy*, 2022, **47**, 12726–12738.

27 S. P. du Preez, D. R. Jones, M. E. A. Warwick, A. Falch, P. T. Sekoai, C. Mota das Neves Quaresma, D. G. Bessarabov and C. W. Dunnill, Thermally stable Pt/Ti mesh catalyst for catalytic hydrogen combustion, *Int. J. Hydrogen Energy*, 2020, **45**, 16851–16864.

28 S. P. du Preez, D. R. Jones, D. G. Bessarabov, A. Falch, C. Mota das Neves Quaresma and C. W. Dunnill, Development of a Pt/stainless steel mesh catalyst and its application in catalytic hydrogen combustion, *Int. J. Hydrogen Energy*, 2019, **44**, 27094–27106.

29 L. M. Botha, C. N. M. Ouma, K. O. Obodo and D. Bessarabov, Hydrogen and oxygen recombination reaction on Pt–Ni and Pt–Co based alloys using density functional theory, *Surf. Sci.*, 2023, **736**, 122354.

30 L. M. Botha, K. O. Obodo, C. N. M. Ouma, D. G. Bessarabov, D. L. Sharypin, P. S. Varyushin and E. I. Plastinina, Density functional theory studies of Pd and Pt_xPd_{1-x} bimetallic catalysts for the H_2/O_2 recombination reaction, *Comput. Mater. Sci.*, 2025, **246**, 113451.

31 D. Qi, X. Luo, Y. Yao, N. Qi, X. Lu, H. Chen and H. Shi, Computational Study of H_2 Catalytic Combustion on Pd_{38} Cluster Model and Pd(111) Slab Model, *Symmetry*, 2022, **14**, 1544.

32 Y. Wang, H. Shao, C. Zhang, F. Liu, J. Zhao, S. Zhu, M. K. H. Leung and J. Hu, Molecular dynamics for electrocatalysis: Mechanism explanation and performance prediction, *Energy Rev.*, 2023, **2**, 100028.

33 H. Hosseini, C. J. Herring, C. F. Nwaokorie, G. A. Sulley and M. M. Montemore, Computational Design of Catalysts with Experimental Validation: Recent Successes, Effective Strategies, and Pitfalls, *J. Phys. Chem. C*, 2024, **128**, 18144–18157.

34 I. Batatia, D. P. Kovács, G. N. C. Simm, C. Ortner and G. Csányi, Higher Order Equivariant Message Passing Neural Networks for Fast and Accurate Force Fields, *arXiv*, 2022, arXiv:2206.07697, DOI: 10.48550/arXiv.2206.07697.

35 H. Yang, C. Hu, Y. Zhou, X. Liu, Y. Shi, J. Li, G. Li, Z. Chen, S. Chen, C. Zeni, M. Horton, R. Pinsler, A. Fowler, D. Zügner, T. Xie, J. Smith, L. Sun, Q. Wang, L. Kong, C. Liu, H. Hao and Z. Lu, MatterSim: A Deep Learning Atomistic Model Across Elements, Temperatures and Pressure, *arXiv*, 2024, arXiv:2405.04967, DOI: 10.48550/arXiv.2405.04967.

36 S. Takamoto, C. Shinagawa, D. Motoki, K. Nakago, W. Li, I. Kurata, T. Watanabe, Y. Yayama, H. Iriguchi, Y. Asano, T. Onodera, T. Ishii, T. Kudo, H. Ono, R. Sawada, R. Ishitani, M. Ong, T. Yamaguchi, T. Kataoka, A. Hayashi, N. Charoenphakdee and T. Ibuka, Towards universal neural network potential for material discovery applicable to arbitrary combination of 45 elements, *Nat. Commun.*, 2022, **13**, 2991.

37 Y. Hinuma, Neural Network Potential Molecular Dynamics Simulations of $(La,Ce,Pr,Nd)_{0.95}(Mg,Zn,Pb,Cd,Ca,Sr,Ba)_{0.05}F_{2.95}$, *Phys. Chem. B*, 2024, **128**, 12171–12178.

38 A. Taborosi, K. Aoki, N. Zettsu, M. Koyama and Y. Nagao, Molecular Dynamics Simulation of Polymer Electrolyte Membrane for Understanding Structure and Proton Conductivity at Various Hydration Levels Using Neural Network Potential, *Macromolecules*, 2025, **58**, 3720–3727.

39 S. Takamoto, D. Okanohara, Q. J. Li and J. Li, Towards universal neural network interatomic potential, *J. Mater.*, 2023, **9**, 447–454.

40 A. Hjorth Larsen, J. Jørgen Mortensen, J. Blomqvist, I. E. Castelli, R. Christensen, M. Dułak, J. Friis, M. N. Groves, B. Hammer, C. Hargus, E. D. Hermes, P. C. Jennings, P. Bjerre Jensen, J. Kermode, J. R. Kitchin, E. Leonhard Kolsbjerg, J. Kubal, K. Kaasbjerg, S. Lysgaard,

J. Bergmann Maronsson, T. Maxson, T. Olsen, L. Pastewka, A. Peterson, C. Rostgaard, J. SchiØtz, O. Schütt, M. Strange, K. S. Thygesen, T. Vegge, L. Vilhelmsen, M. Walter, Z. Zeng and K. W. Jacobsen, The atomic simulation environment - A Python library for working with atoms, *J. Phys.: Condens. Matter*, 2017, **29**, 273002.

41 H. Wang, S. Zhou, K. D. Gilroy, Z. Cai and Y. Xia, Icosahedral nanocrystals of noble metals: Synthesis and applications, *Nano Today*, 2017, **15**, 121–144.

42 S. Nosé, A unified formulation of the constant temperature molecular dynamics methods, *J. Chem. Phys.*, 1984, **81**, 511–519.

43 W. G. Hoover, Canonical dynamics: Equilibrium phase-space distributions, *Phys. Rev. A*, 1985, **31**, 1965–1967.

44 G. Kresse and J. Furthmiiller, Efficiency of ab-initio total energy calculations for metals and semiconductors using a plane-wave basis set, *Comput. Mater. Sci.*, 1996, **6**, 15–50.

45 B. Cordero, V. Gómez, A. E. Platero-Prats, M. Revés, J. Echeverría, E. Cremades, F. Barragán and S. Alvarez, Covalent radii revisited, *RSC Dalton Trans.*, 2008, 2832–2838.

46 A. Plauck, E. E. Stangland, J. A. Dumesic and M. Mavrikakis, Active sites and mechanisms for H_2O_2 decomposition over Pd catalysts, *Proc. Natl. Acad. Sci. U. S. A.*, 2016, **113**, 1973–1982.

47 E. M. Dietze, L. Chen and H. Grönbeck, Surface steps dominate the water formation on Pd(111) surfaces, *J. Chem. Phys.*, 2022, **156**, 064701.

48 T. Jacob, The Mechanism of Forming H_2O from H_2 and O_2 over a Pt Catalyst via Direct Oxygen Reduction, *Fuel Cells*, 2006, **6**, 159–181.

49 J. Greeley and M. Mavrikakis, Surface and Subsurface Hydrogen: Adsorption Properties on Transition Metals and Near-Surface Alloys, *J. Phys. Chem. B*, 2005, **109**, 3460–3471.

50 L. Xu, J. Lin, Y. Bai and M. Mavrikakis, Atomic and Molecular Adsorption on Cu(111), *Top. Catal.*, 2018, **61**, 736–750.

51 T. Pu, A. Setiawan, A. C. Foucher, M. Guo, J.-M. Jehng, M. Zhu, M. E. Ford, E. A. Stach, S. Rangarajan and I. E. Wachs, Revealing the Nature of Active Oxygen Species and Reaction Mechanism of Ethylene Epoxidation by Supported Ag/α-Al_2O_3 Catalysts, *ACS Catal.*, 2024, **14**, 406–417.

52 L. Barrio, P. Liu, J. A. Rodríguez, J. M. Campos-Martín and J. L. G. Fierro, A density functional theory study of the dissociation of H_2 on gold clusters: Importance of fluxionality and ensemble effects, *J. Chem. Phys.*, 2006, **125**, 164715.

53 G. J. Hutchings, Heterogeneous Gold Catalysis, *ACS Cent. Sci.*, 2018, **4**, 1095–1101.

54 S. Seraj, P. Kunal, H. Li, G. Henkelman, S. M. Humphrey and C. J. Werth, PdAu Alloy Nanoparticle Catalysts: Effective Candidates for Nitrite Reduction in Water, *ACS Catal.*, 2017, **7**, 3268–3276.

55 Y. Santiago-Rodríguez, J. A. Herron, M. C. Curet-Arana and M. Mavrikakis, Atomic and molecular adsorption on Au(111), *Surf. Sci.*, 2014, **627**, 57–69.

56 J. A. Herron, S. Tonelli and M. Mavrikakis, Atomic and molecular adsorption on Pd(111), *Surf. Sci.*, 2012, **606**, 1670–1679.

57 B. W. J. Chen, D. Kirvassilis, Y. Bai and M. Mavrikakis, Atomic and Molecular Adsorption on Ag(111), *J. Phys. Chem. C*, 2019, **123**, 7551–7566.

58 D. C. Ford, Y. Xu and M. Mavrikakis, Atomic and molecular adsorption on Pt(111), *Surf. Sci.*, 2005, **587**, 159–174.

59 P. Sabatier, *Catalysis in Organic Chemistry*, Library Press, 1922.

60 J. L. Gland, B. A. Sexton and G. B. Fisher, Oxygen interactions with the Pt(111) surface, *Surf. Sci.*, 1980, **95**, 587–602.

61 R. Naumann d'Alnoncourt, B. Graf, X. Xia and M. Muhler, The back-titration of chemisorbed atomic oxygen on copper by carbon monoxide investigated by microcalorimetry and transient kinetics, *J. Therm. Anal. Calorim.*, 2008, **91**, 173–179.

62 C. T. Campbell, Atomic and molecular oxygen adsorption on Ag(111), *Surf. Sci.*, 1985, **157**, 43–60.

63 N. Saliba, D. H. Parker and B. E. Koel, Adsorption of oxygen on Au(111) by exposure to ozone, *Surf. Sci.*, 1998, **410**, 270–282.

64 K. Christmann, Interaction of hydrogen with solid surfaces, *Surf. Sci. Rep.*, 1988, **9**, 1–163.

65 B. Poelsema, G. Mechtersheimer and G. Comsa, The interaction of hydrogen with platinum(s)−9(111) × (111) studied with helium beam diffraction, *Surf. Sci.*, 1981, **111**, 519–544.

66 G. Lee, P. T. Sprunger, M. Okada, D. B. Poker, D. M. Zehner and E. W. Plummer, Chemisorption of hydrogen on the Ag(111) surface, *J. Vac. Sci. Technol., A*, 1994, **12**, 2119–2123.